QCD@Work 2003 - International Workshop on QCD, Conversano, Italy, 14–18 June 2003

Particle Production, Correlations and Jet Quenching at RHIC

John W. Harris*

Physics Department, Yale University,
P.O. Box 208124, 272 Whitney Avenue, New Haven CT, U.S.A. 06520-8124

Results from RHIC depict formation of a dense system at an energy density greater than 5 GeV/fm^3, well above that where hadrons exist. Statistical models that describe RHIC data indicate a temperature and baryo-chemical potential at the deconfinement phase transition boundary predicted by lattice QCD calculations. The anisotropic collective flow observed in collisions at RHIC provides direct evidence of strong pressure gradients in the highly interacting dense medium. Suppression of hadrons at large transverse momentum, and quenching of di-jets are observed in central Au + Au collisions and provide evidence for large energy loss of partons traversing the dense matter created at RHIC.

1 Introduction

Calculations of Quantum Chromodynamics (QCD) on the lattice predict a deconfinement phase transition from hadrons to a Quark-Gluon Plasma (QGP) and an accompanying chiral phase transition [1,2]. A sharp deconfinement transition occurs at a temperature of approximately 175 MeV in 2-flavor QCD and at about 20 MeV lower temperature for 3-flavors in the chiral limit at zero baryo-chemical potential. There has been recent success in implementation of techniques to calculate on the lattice at a small but finite baryon density [3]. Understanding the nature of these phase transitions is expected to have implications for nuclear physics, astrophysics, cosmology and particle physics.

The Relativistic Heavy Ion Collider (RHIC) was constructed to create the QGP in the laboratory and study its properties. RHIC accelerates and collides ions from protons to the heaviest nuclei over a range of energies, up to 250 GeV for protons and 100 A-GeV for Au nuclei. Since 2000 in the three production runs for physics, RHIC has collided Au + Au at center-of-mass energies $\sqrt{s_{NN}}$ = 19.6, 130, and 200 GeV, d + Au at $\sqrt{s_{NN}}$ = 200 GeV, and p + p at $\sqrt{s}$ = 200 GeV. RHIC has also begun to collide polarized protons for studies of the spin content of the proton. RHIC and its four experiments (BRAHMS, PHENIX, PHOBOS, and STAR) are described comprehensively in [4].

This presentation will describe the experimental search for the QGP at RHIC and will focus on particle production, correlations, and large transverse momentum phenomena. It will be divided into two parts: 1) creating and establishing the properties of the high density matter at RHIC through the study of soft (low transverse momentum) particle production and correlations, and 2) probing the matter with hard (high transverse momentum) probes to determine its response.

*John.Harris@Yale.edu

2 Creating High Density Matter

Many aspects of the matter created at RHIC, such as its bulk properties and collective effects, can be understood by studying the particles most abundantly produced in these collisions, i.e. those with transverse momentum less than 2 GeV/c.

2.1 Particle Production

A large number of particles is produced in a central collision at RHIC. The measured charged hadron multiplicity density at midrapidity is $dn_{ch}/d\eta\ |_{\eta=0}= 700 \pm 27(syst)$ [5] for the 3% most central collisions of Au + Au at $\sqrt{s_{NN}}$ = 200 GeV. This corresponds to a hadron multiplicity density $dn_{total}/d\eta\ |_{\eta=0}$= 1050 and a total hadron multiplicity in the most central events of $\sim$ 7000 [5,6]. In terms of number of quarks, consider the case where all observed hadrons in the final state are mesons, each containing a quark and anti-quark. Thus, 7,000 hadrons correspond to 14,000 quarks and anti-quarks. A lower limit for the number of produced quarks and anti-quarks can be obtained by subtracting off the valence quarks that originally enter the collision in the incident nuclei. The number of valence quarks in a head-on collision of two Au nuclei is 2 (Au nuclei) x 197 nucleons per Au x 3 quarks per nucleon $\sim$ 1200. Thus, more than 90% of the more than 14,000 quarks and anti-quarks in the final state are produced in the collision. In addition, there are a large number of gluons present that have not been considered in this simple estimate.

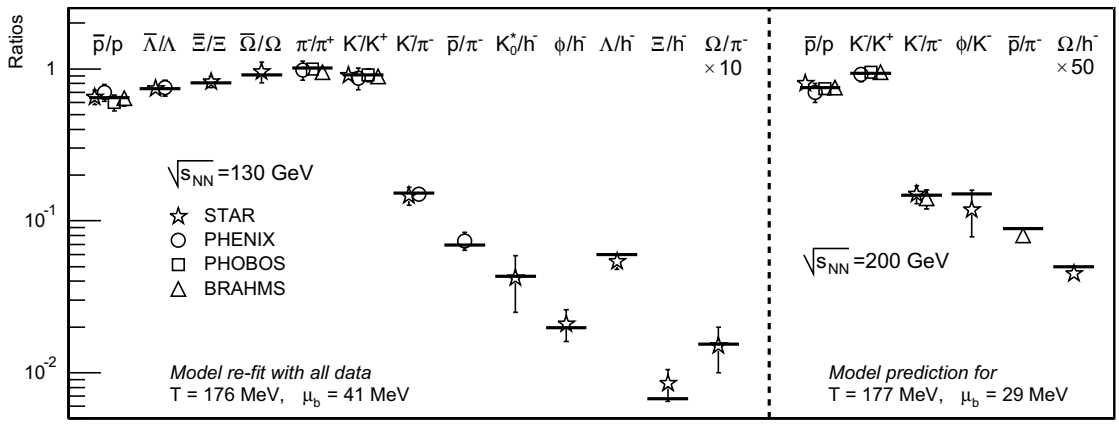

Figure 1. Particle ratios (defined at top) measured in RHIC experiments (denoted by various symbols and defined in the legend) along with statistical-thermal model predictions (horizontal dashes) [11] for central collisions of Au + Au at $\sqrt{s_{NN}}$ = 130 (left) and 200 GeV (right).

2.2 Energy Density

Large energy densities are reached in a central collision at RHIC. Measurements of the transverse energy per unit pseudorapidity $dE_T/d\eta$ [7] or the total particle multiplicity density and mean transverse momentum per particle [8] can be used to estimate the energy density produced in a Bjorken longitudinal expansion scenario [9].

In Au + Au collisions at $\sqrt{s_{NN}}$ = 130 GeV there is longitudinal boost invariance in a region around mid-rapidity at RHIC [8]. Here the Bjorken scenario applies and the energy density can be estimated by $\epsilon_{Bj} = \frac{1}{\tau_o \pi R^2} \times \frac{dE_T}{dy}$, with dE_T/dy the transverse energy per unit rapidity, R the transverse radius of the system, and τ_o the formation time. Assuming a maximum value for the formation time τ_o = 1 fm/c, the minimum energy density for central collisions of Au + Au at $\sqrt{s_{NN}}$ = 130 GeV is 4.6 GeV/fm^3 for the 2% most central Au + Au collisions [7] and 4.3 GeV/fm^3 for the 5% most central Au + Au collisions [8]. This is a 60% increase over the value 2.9 GeV/fm^3 measured for Pb + Pb at $\sqrt{s_{NN}}$ = 17.2 GeV at the CERN SPS. Note that the value for τ_o is expected to be significantly smaller at RHIC than at the SPS, thus the energy density derived for RHIC from this formula is a minimum and may be significantly ($\sim$ ten times) larger.

2.3 Hadronization and Quark Coalescence

Measurements of the ratios of various types of particles provide insight into aspects of the hadronization process. A particle formation mechanism involving the coalescence of quarks [10], predicts that these ratios should have specific relationships that are determined strictly from combining the various types of quarks that make up the observed particles. The measured values of the particle ratios $\bar{p}/p$, $\bar{\Lambda}/\Lambda$, $\bar{\Xi}/\Xi$ and $\bar{\Omega}/\Omega$ at mid-rapidity are reproduced using the measured value of K^+/K^- and the coalescence formulae [10], indicating that the particle formation mechanism involves coalescence of quarks with little or insignificant rescattering after the particle ratios are established.

2.4 Temperature and Baryo-Chemical Potential

By comparing the ratios of the many different types of particles measured in RHIC collisions, properties of the system at chemical freeze-out can be established. Ratios of the numbers of anti-particles to particles are sensitive to the net baryon number density. Likewise, measurement of the total number of produced particles and ratios of non-identical particles provide information on the temperature of the system when the particles are formed. The results of a thermal model comparison [11] to the measured particle ratios are displayed in Fig. 1 for Au + Au at $\sqrt{s_{NN}}$ = 130 and 200 GeV (left and right panels). The best global fits for central collisions of Au + Au at $\sqrt{s_{NN}}$ = 130 and 200 GeV are (T, μ_B) = (176 MeV, 41 MeV) and (177 MeV, 29 MeV), respectively. These values are in good agreement with other thermal model analyses and are at the deconfinement phase boundary. This is seen in Fig. 2, which is a compilation [12] of (T, μ_B) points derived from thermal model analyses of experimental results at various energies. The data and thermal model systematics in conjunction with the lattice QCD calculations (see Fig. 2) indicate that at chemical freezeout the system at RHIC is at the phase boundary.

2.5 Collective Effects - Radial Flow

The transverse momentum spectra of hadrons provide information about the system at the time of thermal

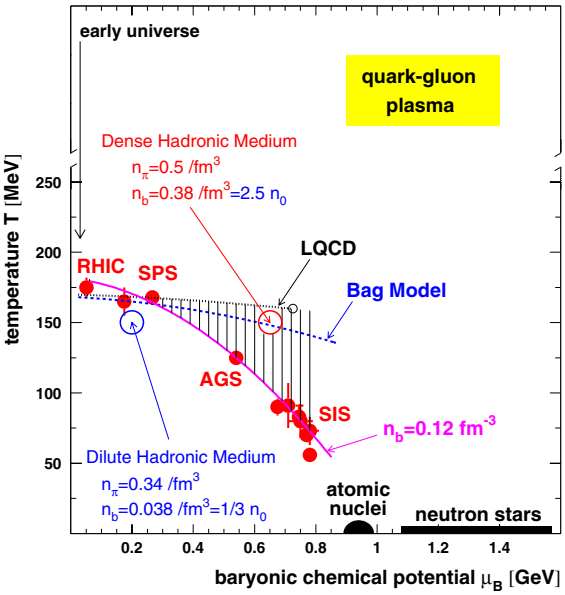

Figure 2. Nuclear phase diagram extracted from a thermal model analysis of experimental results at various energies and heavy ion facilities (SIS, AGS, SPS, and RHIC) [12]. The dotted curve labeled "LQCD" corresponds to the deconfinement phase boundary predicted by lattice QCD [14]. The solid curve corresponds to freeze-out at a constant baryon density.

freeze-out, when interactions cease, while also containing a history of the expansion process and any collective effects. Displayed in Fig. 3 are the transverse momentum spectra measured for charged pions, kaons and anti-protons in $\sqrt{s_{NN}}$ = 200 GeV Au + Au central collisions. Also, shown are the results of a hydrodynamics calculation [13] that incorporates a quark-gluon to hadron phase transition at T_c = 165 MeV, and subsequent hydrodynamic expansion in a hadronic phase in chemical equilibrium including effective meson and baryon chemical potentials. In this calculation, pre-equilibrium collective flow at the time of thermalization is required to fit the spectra of the particles at the top RHIC energy.

2.6 Collective Effects - Elliptic Flow

Non-zero impact parameter collisions have an inherent initial spatial asymmetry in the plane perpendicular to the beam axis due to the impact parameter. The larger the impact parameter the larger the asymmetry. If the initial spatial asymmetry is transferred into a momentum-space anisotropy during the brief traversal time of the incident nuclei ($\sim$ 1 fm/c at these energies), the resulting azimuthal asymmetry is evidence for the presence of large pressure gradients early in the collision process and requires a dense, highly interacting medium.

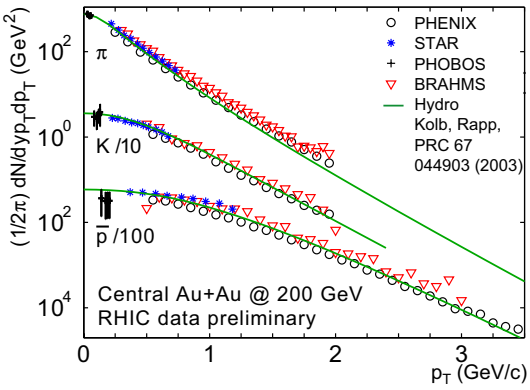

Figure 3. Transverse momentum spectra of charged pions, kaons and anti-protons measured in $\sqrt{s_{NN}}$ = 200 GeV Au + Au central collisions. Shown as the curves are the results of a hydrodynamics calculation [13].

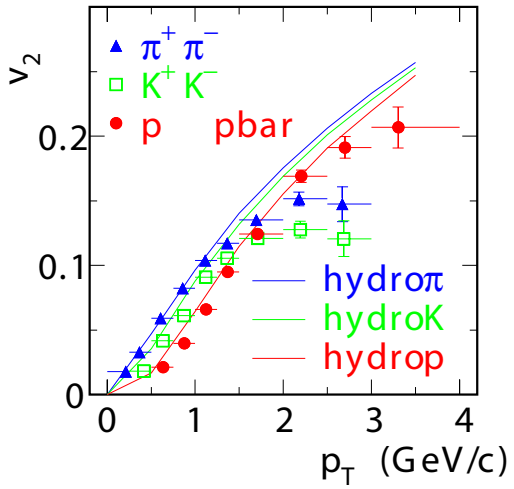

Figure 4. Measured elliptic flow v_2 for $\sqrt{s_{NN}}$ = 200 GeV Au + Au minimum bias collisions as a function of p_T for $\pi^\pm$, $K^\pm$, and $p^\pm$ from PHENIX [15]. Curves are hydrodynamics predictions. [17,18]

A way to measure the azimuthal asymmetry is to construct the second Fourier harmonic component of the azimuthal distribution of particles in momentum space with respect to the reaction plane, $v_2 = \langle\cos(2\phi)\rangle$ where ϕ = atan (p_y/p_x). This v_2 is called the elliptic flow. Displayed in Figs. 4, 5 are v_2 measured by PHENIX [15] for $\pi^\pm$, $K^\pm$, and $p^\pm$ and by STAR [16] for K^o_s, $\Lambda + \overline{\Lambda}$,$(h^+ + h^-)/2$, respectively, as a function of transverse momentum in $\sqrt{s_{NN}}$ = 200 GeV Au + Au minimum bias collisions. Also shown are predictions from hydrodynamics. The elliptic flow is well described at low transverse momenta by hydrodynamical models incorporating a softening of the equa-

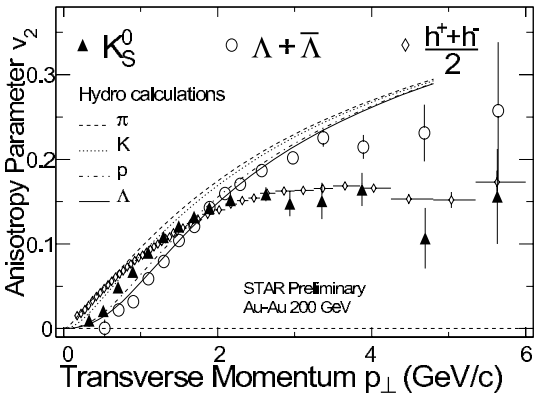

Figure 5. Measured elliptic flow v_2 for $\sqrt{s_{NN}} = 200$ GeV Au + Au minimum bias collisions as a function of p_T for $K^o{}_s$, $\Lambda + \overline{\Lambda}$, and $(h^+ + h^-)/2$ from STAR. [16] Curves are hydrodynamics predictions. [17,18]

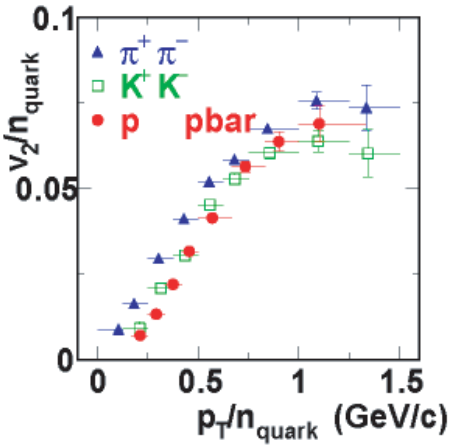

Figure 6. v_2 per quark as a function of p_T per quark for $\sqrt{s_{NN}} = 200$ GeV Au + Au minimum bias collisions for $\pi^{\pm}$, $K^{\pm}$, and $p^{\pm}$ from PHENIX [15].

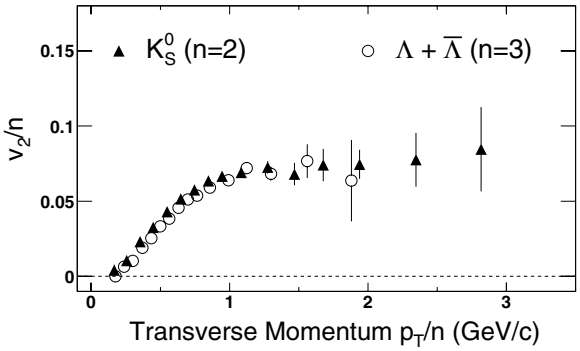

Figure 7. v_2 per quark as a function of p_T per quark for $\sqrt{s_{NN}} = 200$ GeV Au + Au minimum bias collisions for $K^o{}_s$, $\Lambda + \overline{\Lambda}$, and $(h^+ + h^-)/2$ from STAR [16].

tion of state due to quark and gluon degrees of freedom [17,18]. However, at transverse momenta > 1.5 GeV/c the lighter particles (π, K) deviate from the predictions of hydrodynamics as do the heavier particles (p, Λ) at slightly higher transverse momenta. The baryons continue to have higher values of v_2 than the mesons at the largest transverse momenta measured. The saturation of v_2 for larger momenta reflects effects of the energy loss due to the large gluon densities of the evolving medium [19].

Larger values of v_2 for baryons than mesons at larger transverse momenta may result from the particles being created in soft processes and promoted to higher p_T by a collective boost. Alternatively or in addition, coalescence or recombination of quarks to form composite particles may occur. In this scenario, the elliptic flow per quark (v_2/n_{quarks}) should be the same for all particles when plotted as a function of the transverse momentum per quark (p_T/n_{quarks}), where n_{quarks} is the number of quarks in each particle. Displayed in Figs. 6, 7 are v_2/n_{quarks} as a function of p_T/n_{quarks}. The PHENIX results on $\pi^{\pm}$, $K^{\pm}$, and $p + \overline{p}$ are plotted per quark in Fig. 6. The STAR results for $K^o{}_s$ and $\Lambda + \overline{\Lambda}$ per quark are plotted in Fig. 7. The v_2/n_{quarks} scales (overlays) for the various particles when plotted versus p_T/n_{quarks} for quark $p_T > 1.0$ GeV/c. These data are consistent with a quark coalescence picture for strange hadrons with quark $p_T > 1.0$ GeV/c. See [20] for further discussion.

3 Using Hard-Scattering to Probe the Medium

For the first time in relativistic heavy ion collisions, hard scattering has been used at RHIC to probe the medium through which the hard-scattered partons propagate. The radiation energy loss of a parton traversing a dense medium is predicted to be significant and is sensitive to the gluon density of the medium [21–23]. In order to investigate parton energy loss in the medium, the RHIC experiments have measured hadron spectra and azimuthal correlations of particles with large transverse momentum.

3.1 Hadron Spectra at Large Transverse Momentum

In order to investigate parton energy loss, initially PHENIX and STAR measured hadron spectra at large transverse momentum in Au + Au collisions at $\sqrt{s_{NN}} = 130$ GeV. Both groups reported significant suppression of hadron production at transverse momenta $2 < p_T < 6$ GeV/c [24,25] relative to elementary collisions, and normalized to the number of binary collisions.

New data on hadron transverse momentum distribu-

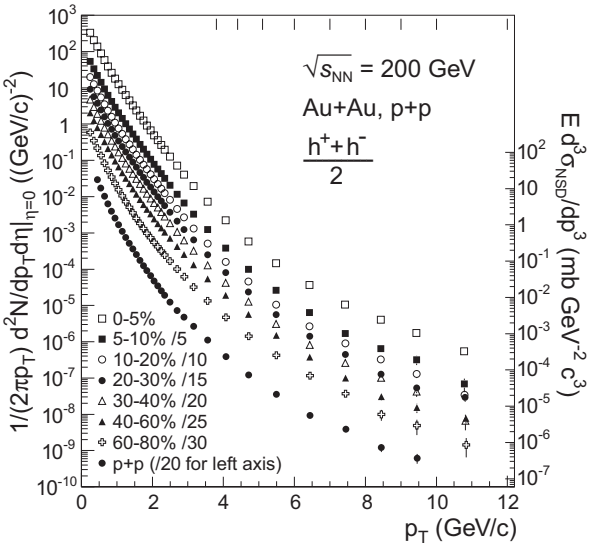

Figure 8. Charged hadron spectra for $\sqrt{s_{NN}} = 200$ GeV Au + Au collisions (left axis) for various centralities and for non-single-diffractive p + p collisions (right axis) from STAR [26].

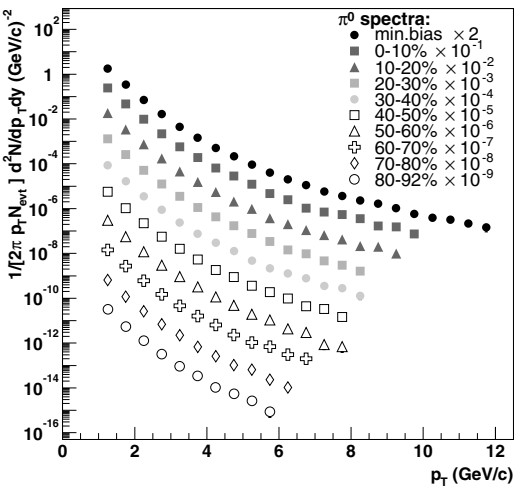

Figure 9. π^o yields as a function of p_T measured at midrapidity in $\sqrt{s_{NN}} = 200$ GeV Au + Au collisions from PHENIX [27]. Displayed are minimum bias collisions and various centralities (shown in the legend).

tions at the top energy of RHIC, $\sqrt{s_{NN}} = 200$ GeV, from STAR in Au + Au collisions are displayed in Fig. 8 as a function of collision centrality [26]. Also, shown are non-single-diffractive data from p + p interactions. These new data extend over nine orders of magnitude in cross section out to 12 GeV/c transverse momentum. PHENIX has measured π^o production over the same range of p_T and centralities in $\sqrt{s_{NN}} = 200$ GeV Au + Au [27]. The PHENIX data are shown in Fig. 9. These data will be examined and discussed in more detail in the next section.

3.2 Suppression of Particles with Large Transverse Momenta

In order to make comparisons of results from collisions of nuclei with those of elementary particles, such as p + p, a nuclear modification factor can be defined as $R_{AA}(p_T) = \frac{dN^2/dp_T dy\ (AA)}{\langle N_{binary}\rangle dN^2/dp_T dy\ (NN)}$. $\langle N_{binary}\rangle$ is the number of binary collisions in a geometrical model used to scale from elementary nucleon-nucleon (NN) collisions to nucleus-nucleus (AA) collisions. $R_{AA} = 1$ when AA is an incoherent superposition of NN collisions corresponding to scaling with the number of binary collisions (binary scaling).

Deviations from binary scaling are observed in the nuclear modification factors measured at RHIC. Displayed in Fig. 10 is the π^o nuclear modification factor as a function of transverse momentum for the peripheral and central Au + Au collision data from PHENIX [27]. The ratios are taken relative to p + p collisions scaled by the number of binary collisions. The peripheral collision data exhibit no nuclear modification, i.e. $R_{AA} = 1$, within errors, whereas the central collision data are suppressed by about a factor of five relative to the pQCD expectation. The charged hadron data of STAR are shown in Fig. 11 for collisions of Au + Au relative to p + p collisions for six centrality bins as labelled in the panels [26]. These data exhibit a clear suppression that increases with increasing centrality reaching a factor of 4 - 5 for the most central collisions. The ratio remains rather flat up to the statistical limits of the data at 10 GeV/c transverse momentum, where no sign of reaching the pQCD limit of binary scaling is yet seen. Also displayed in Fig. 11 as gray bands (and labelled) are Glauber calculations and uncertainties for binary and participant scaling. Full p-QCD calculations (denoted p-QCD-I [28]) including influences of nuclear effects (shadowing and Cronin, as labelled) are shown in Fig. 11. It is seen that the shadowing and Cronin enhancement cannot account for the suppression in the data. Only after inclusion of partonic energy loss in a dense medium with ~ 15 times the energy loss of cold nuclear matter, can the data be fit. Also shown for comparison are full p-QCD (p-QCD-II) calculations with parton energy loss from [29].

The modification factors measured for heavy ions at SPS energies rise as a function of p_T, exceed 1 above $p_T \sim 1.5$ GeV/c, and remain above 1 up to the highest p_T measured (4 GeV/c). This excess has been described in terms of an anomalous nuclear enhancement, an initial state (Cronin) effect [30]. However, no energy loss or quenching effects due to the medium have been observed in the hadron spectra from the

SPS.

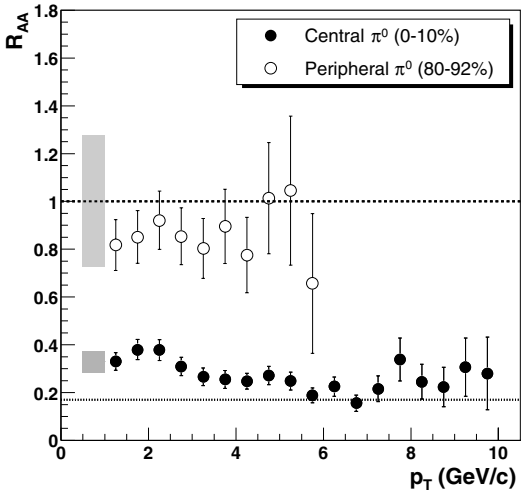

Figure 10. The π^o nuclear modification factors plotted for peripheral and central Au + Au collisions at $\sqrt{s_{NN}}$ = 200 GeV relative to p + p interactions from PHENIX [27]. Error bars are statistical plus systematic, while the shaded regions represent the errors on normalization of the ratios.

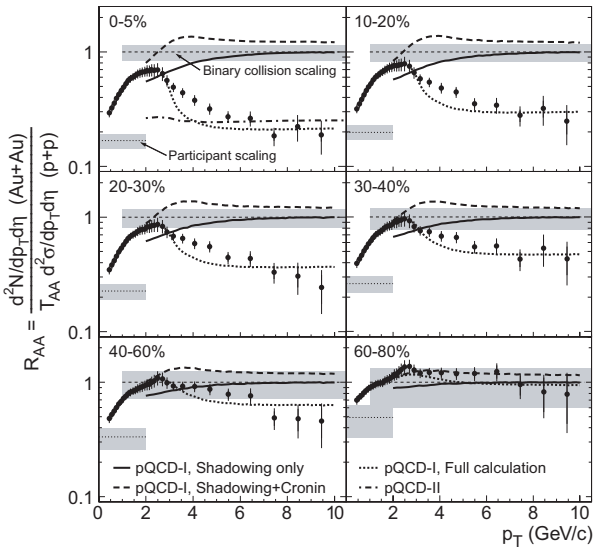

Figure 11. Nuclear modification factors R_{AA} as a function of transverse momentum for charged hadrons. Plotted are six centrality bins for Au + Au collisions at $\sqrt{s_{NN}}$ = 200 GeV relative to p + p interactions from STAR [26]. See text for details.

The suppression of the hadron spectra at large transverse momenta that is observed in central Au + Au collisions at RHIC [24,25] may result from a combination of initial and final state effects. To distinguish initial and final state effects, measurements were carried out using d + Au interactions for comparison to p + p and Au + Au at RHIC. Displayed in Figs. 12,13 are the nuclear modification factors as a function of transverse momentum for central Au + Au collision data and for d + Au collisions from PHENIX [31] and STAR [32], respectively. The ratios are taken relative to p + p collisions scaled by the number of binary collisions. These data exhibit a clear suppression by a factor 4-5 in the central Au + Au case. The central Au + Au ratio remains rather flat up to the statistical limits of the data at 10 GeV/c transverse momentum, where no sign of reaching the pQCD limit of binary scaling is observed. The peripheral collision data (seen in Figs. 10,11) exhibit no nuclear modification, i.e. $R_{AA} = 1$, within errors. The Au + Au relative to p + p yields are reproduced by pQCD calculations incorporating parton energy loss in dense matter [33] and by a model incorporating initial-state gluon saturation [34]. The ratio $R_{dAu}(p_T) > 1$ in d + Au reflects a Cronin enhancement (initial state multiple scattering) for 1 $< p_T <$ 7 GeV/c and no suppression, rather a slight enhancement. The d + Au charged hadron data when compared to scaled p + p data [31,32,35,36] rule out initial-state gluon saturation leaving only final state effects as a cause of the suppression in the Au + Au data at mid-rapidity at RHIC.

Displayed in the top panel of Fig. 14 are the ratios of $K^o{}_s$, $\Lambda + \overline{\Lambda}$, and $(h^+ + h^-)/2$ produced in central relative to binary-scaled peripheral collisions. [37] The $K^o{}_s$ and $(h^+ + h^-)/2$ ratio of central to peripheral peak around $p_T \sim 1.5$ GeV/c at ratios considerably below 1 and continue to be suppressed up to $p_T \sim 6$ GeV/c. The ratios of central to peripheral yields of $\Lambda + \overline{\Lambda}$ peak near unity and are suppressed relative to binary-scaling only above around 4 GeV/c. For comparison, the PHENIX data on π^o and $p + \overline{p}$ are shown in the bottom panel of Fig. 14 [38]. The π^o are suppressed by a factor of $\sim$ 4 - 5, while the protons do not deviate from binary scaling up to transverse momentum 4 GeV/c.

While the baryons (p, Λ) exhibit a larger elliptic flow compared to the mesons (π, K), they are not as suppressed as the mesons. If energy loss is the basis for elliptic flow at high p_T, one would expect that particles exhibiting large suppression in the high p_T spectra (e.g. π, K) will also have larger elliptic flow. But this is not the case, presenting a dilemma.

3.3 Jet Quenching of Azimuthal Correlations at Large Transverse Momenta

Due to the complexities of identifying and determining precisely the energies of jets in the large background of soft particles in relativistic heavy ion collisions, two-particle correlations of large transverse momentum hadrons can be used to identify the hard scattering component on a statistical basis.

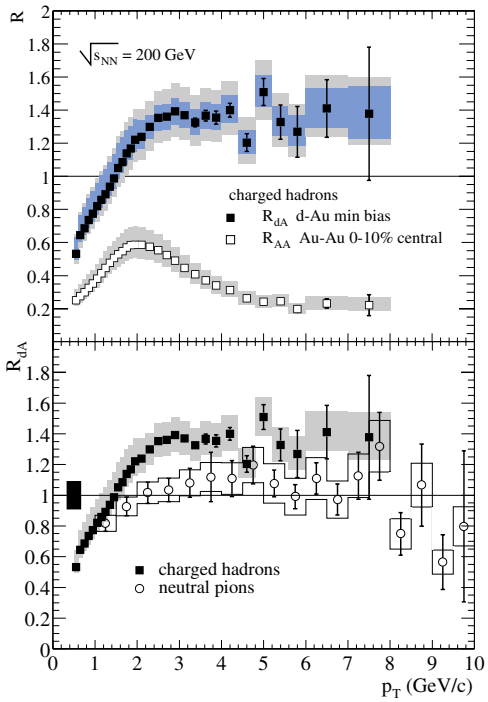

Figure 12. Nuclear modification factor for $\sqrt{s_{NN}} = 200$ GeV minimum bias d + Au and for central Au + Au from PHENIX [31] for charged hadrons and neutral pions.

The fragmentation of partons should lead to jets, a correlation of hadrons in a small angular region of relative azimuthal angle ($\Delta\phi$) and pseudorapidity ($\Delta\eta$). As seen in Fig. 15 an enhancement is observed at $\Delta\phi = 0$ in azimuthal correlations near midrapidity upon correlating charged hadrons having $4 < p_T^{trig} < 6$ GeV/c with all other charged hadrons having 2 GeV/c $< p_T < p_T^{trig}$ in the same event. This has been seen in collisions of Au + Au at $\sqrt{s_{NN}} = 130$ and 200 GeV ranging from minimum bias to central collisions, and in p + p and d + Au at $\sqrt{s} = 200$ GeV [39,40]. The peak at small relative azimuthal angle is indicative of short range correlations and suggests contributions from jets and/or resonance decays. The p + p, d + Au, and peripheral Au + Au data exhibit a distinct back-to-back correlation, a characteristic of hard-parton scattering, with peaks at $\Delta\phi = 0$ and π, indicating di-jets. This is shown in Fig. 15 for the p + p and d + Au reactions, whereas for the most central Au + Au collisions the backward ($\Delta\phi = \pi$) correlation disappears. These results indicate that strong dissipative effects of the medium created in central Au + Au collisions quench high momentum partons or their fragmentation products, and provide further evidence that the suppression at large p_T in the spectra is not a product of initial state gluon saturation.

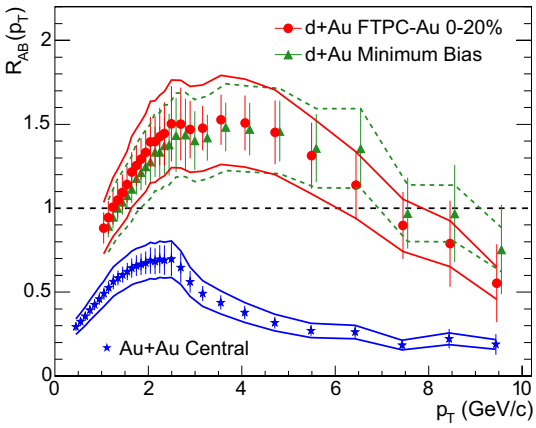

Figure 13. Nuclear modification factor for $\sqrt{s_{NN}} = 200$ GeV for charged hadrons in minimum bias d + Au and central d + Au and Au + Au from STAR [32].

4 Conclusions and Outlook

Results from RHIC depict the formation of a dense system at an energy density greater than 5 GeV/fm^3, well above that where hadrons can exist. As the system evolves it can be described by the coalescence of quarks and subsequently by statistical models that indicate a temperature and baryo-chemical potential at the deconfinement phase transition boundary predicted by lattice QCD calculations. Collective flow is observed and provides direct evidence of strong pressure gradients in a highly interacting dense medium. Hard-scattering, suppression of hadrons at large transverse momentum, and quenching of di-jets are observed providing evidence for extreme energy loss of partons or their fragmentation products propagating in the hot matter created at RHIC.

References

1. see F. Karsch, Nuc. Phys. A698 (2002) 199c.
2. see K. Kanaya, Nuc. Phys. A715 (2003) 233c.
3. see Z. Fodor, Nuc. Phys. A715 (2003) 319c.
4. Nuc. Inst. Meth. A499 (2003) p. 235-824.
5. B. Back et al (PHOBOS), Phys. Rev. C65 (2002) 061901R.
6. B. Back et al (PHOBOS), Phys. Rev. Lett. 87 (2001) 102303.
7. K. Adcox et al. (PHENIX) Phys. Rev. Lett. 87 (2001) 052301.
8. C. Adler et al. (STAR), Phys. Rev. Lett. 87 (2001) 112303.
9. J.D. Bjorken, Phys. Rev. D27 (1983) 140.
10. T.S. Biro, P. Levai and J. Zimanyi, Phys. Lett. B347 (1995) 6.

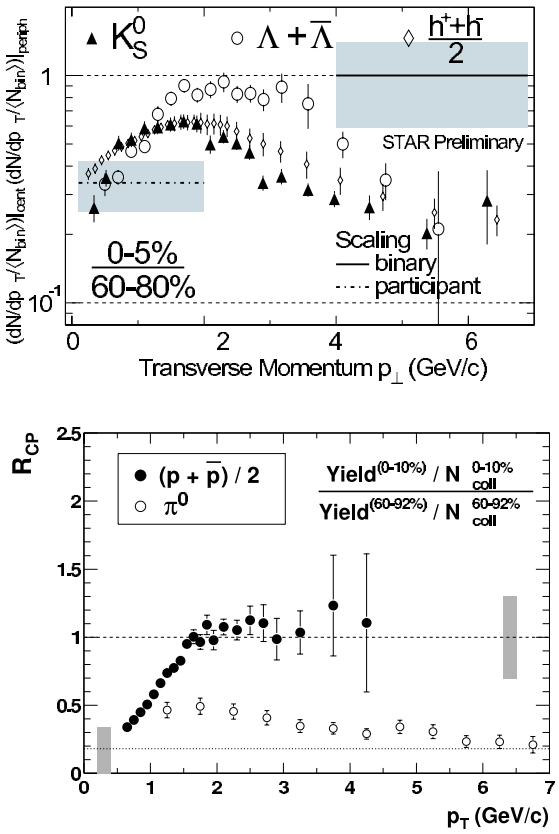

Figure 14. $\sqrt{s_{NN}}$ = 200 GeV Au + Au collision data for ratios of $K^o{}_s$, Λ, $\bar{\Lambda}$, and $(h^+ + h^-)$ / 2 (top panel) from STAR [37] and π^o and $(p+\bar{p})/2$ (bottom panel) from PHENIX [38].

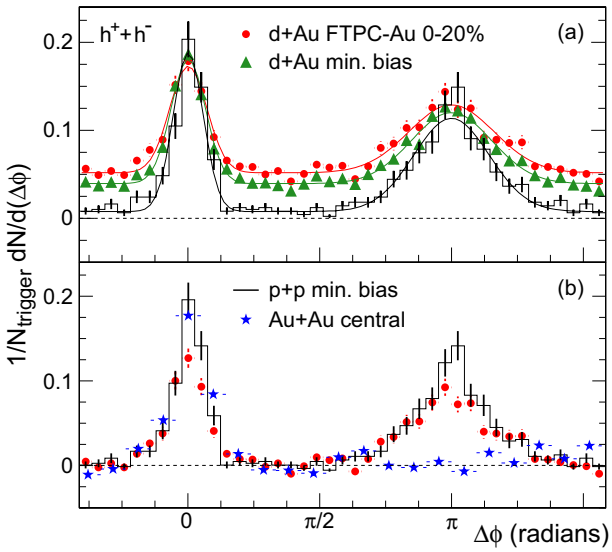

Figure 15. a) Correlation functions in relative azimuth for p + p interactions, and minimum bias and central collisions of d + Au at $\sqrt{s_{NN}}$ = 200 GeV [40]. b) Comparison of correlations for p + p, central d + Au, and central Au + Au collisions with pedestals subtracted.

Annu. Rev. Part. Sci. 50 (2000) 37.
24. K. Adcox et al (PHENIX), Phys. Rev. Lett. 88 (2002) 022301.
25. C. Adler et al (STAR), Phys. Rev. Lett. 89 (2002) 202301.
26. J. Adams et al (STAR), Phys. Rev. Lett. 91 (2003) 172302.
27. S.S.Adler et al., Phys. Rev. Lett. 91, 072301 (2003).
28. X.N. Wang, nucl-th/0305010.
29. I. Vitev and M. Gyulassy, Phys. Rev. Lett. 89 (2002) 252301.
30. J.W. Cronin et al., Phys. Rev. D11, 3105 (1975); L. Kluberg et al. Phys. Rev. Lett. 38, 670 (1997).
31. K. Adcox et al (PHENIX), Phys. Rev. Lett. 91 (2003) 072303.
32. J. Adams et al (STAR), Phys. Rev. Lett. 91 (2003) 072304.
33. I. Vitev and M. Gyulassy, Phys. Rev. Lett. 89 (2002) 252301.
34. D. Kharzeev et al, Phys. Lett. 561 (2003) 93.
35. B.B. Back et al. (PHOBOS), Phys. Rev. Lett. 91 (2003) 072302.
36. I. Arsene et al. (BRAHMS), Phys. Rev. Lett. 91 (2003) 072305.
37. J. Adams et al (STAR), nucl-ex/0306007.
38. S.S. Adler et al (PHENIX), nucl-ex/0307022.
39. C. Adler et al. (STAR) Phys. Rev. Lett. 90 (2003) 032301.
40. C. Adler et al. (STAR) Phys. Rev. Lett. 89 (2002) 202301.

11. P. Braun-Munzinger, D. Magestro, K. Redlich, and J. Stachel, Phys. Lett. B518 (2001) 41 and D. Magestro (private communication).
12. P. Braun-Munzinger and J. Stachel, nucl-th/0112051 (2001).
13. P. Kolb and R. Rapp, Phys. Rev. C 67 (2003) 044903.
14. Z. Fodor and S.D. Katz, preprint hep-lat/0106002 (2001).
15. S.S. Adler et al (PHENIX), nucl-ex/0305013.
16. J. Adams et al (STAR), nucl-ex/0306007.
17. P.F. Kolb et al., Phys. Lett. B500 (2001) 232; P.F. Kolb et al., Nucl. Phys. A696 (2001) 197.
18. P. Huovinen et al., Phys. Lett. B 503 (2001) 58.
19. M. Gyulassy, I. Vitev, and X.N. Wang, Phys. Rev. Lett. 86 (2001) 2537.
20. C. Nonaka, R. Fries, and S. Bass, nucl-th/0308051.
21. M. Gyulassy and M. Plümer, Phys. Lett. B243 (1990) 432.
22. X. N. Wang and M. Gyulassy, Phys. Rev. Lett. 68 (1992) 1480.
23. R. Baier, D. Schiff, and B. G. Zakharov,